Investigation of microstructure and texture evolution of a Mg/Al laminated composite elaborated by accumulative roll bonding

Walid Habila, Hiba Azzeddine, Brahim Mehdi, Kamel Tirsatine, Thierry Baudin, Anne-Laure Helbert, François Brisset, Sébastien Gautrot, Marie-Hélène Mathon, Djamel Bradai

Materials Characterization 147 (2019) 242–252

Contents lists available at ScienceDirect

Materials Characterization

journal homepage: www.elsevier.com/locate/matchar

Investigation of microstructure and texture evolution of a Mg/Al laminated composite elaborated by accumulative roll bonding

Walid Habila[a], Hiba Azzeddine[a,b,*], Brahim Mehdi[a], Kamel Tirsatine[a], Thierry Baudin[c], Anne-Laure Helbert[c], François Brisset[c], Sébastien Gautrot[d], Marie-Hélène Mathon[d], Djamel Bradai[a]

[a] Faculty of Physics, University of Sciences and Technology Houari Boumediene, BP 32 El-Alia, 16111 Algiers, Algeria.
[b] Departments of Physics, University Mohamed Boudiaf, BP 166, 28000 M'Sila, Algeria
[c] ICMMO, SP2M, Univ. Paris-Sud, Université Paris-Saclay, UMR CNRS 8182, 91405 Orsay Cedex, France
[d] Laboratoire Léon Brillouin, CEA-CNRS, CEA/Saclay, 91191 Gif-sur-Yvette, France.

ARTICLE INFO

Keywords:
Laminated composite
AZ31
Al1050
accumulative roll bonding
microstructure
texture

ABSTRACT

The microstructure and texture of an Al1050/AZ31/Al1050 laminated composite fabricated by accumulative roll bonding at 400 °C up to 5 cycles are investigated using Electron BackScatter Diffraction, neutron diffraction, microhardness measurements and tensile tests. EBSD analysis has shown that ARB processing led to microstructural refinement with equiaxed grain microstructure in AZ31 layers and to the development of elongated grains parallel to the rolling direction in Al 1050 layers. No new phases formed at the bond interface after the first ARB cycle while $Mg_{17}Al_{12}$ and Mg_2Al_3 phases appeared after subsequent cycles. During the ARB processing, a typical strong basal (0002) texture is observed in AZ31 layers along with a weak rolling texture showed in Al 1050 layers with a dominant Rotated Cube {001}⟨110⟩ component. The microhardness of Al1050/AZ31/Al1050 laminated composite increased with increasing ARB cycles and almost saturated after five ARB cycles. The yield strength and ultimate strength increased gradually between 1 and 3 ARB cycles due to the strain hardening and grain refinement. They decreased with further increasing of the ARB cycles because of crack and failure of the Mg_xAl_y intermetallic compounds which developed during 4th and 5th ARB cycles. The deformation behavior of the laminated composite becomes rather similar to the behavior of AZ31 alloy that underwent a dynamic recrystallization during processing.

1. Introduction

Magnesium and Aluminum alloys are used as lightweight materials in aerospace, automotive and as biomaterials due to their lower density among all common structural materials ($\rho_{Mg} = 1.73\,g\,cm^{-3}$, $\rho_{Al} = 2.69\,g\,cm^{-3}$) [1]. However, the use of Magnesium alloys as structural materials is somewhat limited comparatively to Aluminum ones because of their poor workability, low strength and poor corrosion resistance [2]. It has been shown that Aluminum as an alloying element could improve the sheet formability by modification of the final texture [3], enhance the strength through solid solution effect and develop the corrosion resistance of Magnesium [1]. Moreover, it has been reported that introducing an aluminum layer on the surface of magnesium as Al/Mg laminated composite could enhance the corrosion resistance of Magnesium alloy and could combine the excellent properties of both metals [4,5].

Based on thermo-mechanical processing, various techniques have been developed to elaborate multilayered composites through conventional deformation like hot rolling [6–9], hot pressing [10] and twin-roll casting [11]. Recently, severe plastic deformation (SPD) processing such as equal channel angular extrusion (ECAP) [12], high-pressure torsion (HPT) [13] and accumulative roll bonding (ARB) [5,14–20] have been successfully used to produce Al/Mg laminated composites. Particularly, ARB processing may be the most promising SPD process and bears a good potential for commercialization owing to its ability to produce ultra-fine grain (UFG) materials continuously [21].

The evolution of the microstructure at the bond interface of the Al/Mg/Al multilayers and their mechanical properties have been widely investigated [5–9,14–17]. However, in the literature, very few studies do exist either on the crystallographic texture evolution [18,19] or on the microstructure features (interface features, grain size, grain boundary character distribution (GBCD) and dislocation density) of Mg

* Corresponding author.
E-mail address: azehibou@yahoo.fr (H. Azzeddine).

https://doi.org/10.1016/j.matchar.2018.11.010
Received 2 July 2018; Received in revised form 1 November 2018; Accepted 5 November 2018
Available online 07 November 2018

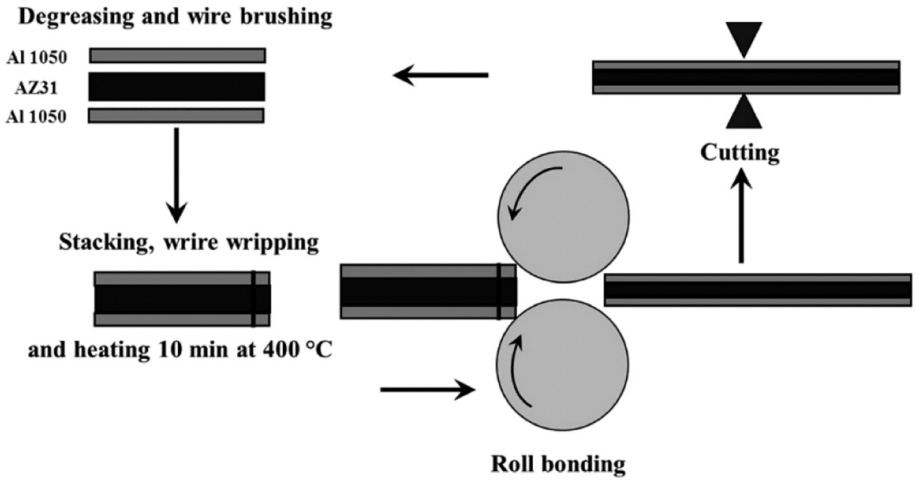

Fig. 1. Scheme of ARB processing.

and Al layers upon increasing ARB cycles [20].

Therefore, the purpose of the present work is to investigate, in detail, the microstructure and texture evolution of both AZ31 and Al1050 layers of the Al1050/AZ31/Al1050 laminated composite fabricated by ARB processing at 400 °C upon increasing ARB cycles using Electron BackScatter Diffraction (EBSD)analysis and neutron diffraction. Phase formation has been investigated by X-ray diffraction. The mechanical properties of Al1050/AZ31/Al1050 composite were analyzed using Vickers microhardness and tensile tests.

2. Experimental Procedure

The materials used in the present work were commercial AZ31 and Al1050 alloys, respectively. The AZ31 (Mg–3Al–1Zn, wt%) sheets with 2 mm thickness were kindly supplied by MagIC - Magnesium Innovations Center, Germany. The Al1050 (AA1050 H18) alloy sheets with 1 mm thickness were supplied by PIMA (Produits Industriels et Métallurgiques SARL, Algeria) Society, Algeria. The principle of ARB processing is illustrated in Fig. 1. Both AZ31 and Al 1050 alloys were cut into 50 × 25 mm rectangular pieces, degreased in acetone and were brushed to remove the surface oxide film and achieve a good bonding.

As shown in Fig. 1, the AZ31 and the Al 1050 alloy sheets were stacked on the treated surface as sequence of Al 1050/AZ31/Al1050 and held at 400 °C for 10 min in a preheated furnace and then warm roll-bonded by applying a large thickness reduction of 50% in a single cycle without any lubricant. The sheets were water-cooled directly after roll-bonding and then cut in halves to start the second cycle. This procedure was repeated up to 5 cycles.

The microstructure of ARB samples were investigated using EBSD in the (Rolling Direction (RD)-Normal Direction (ND)) cross-section after mechanical polishing using SiC papers up to grid 4000 then subsequently with a diamond suspension down to 1/4 of micron. Metallographic preparation was finished by ionic polishing. Samples were positioned in a Gatan PECS II system using the planar mode for thecross sectional EBSD acquisitions. The high voltage was set to 5 kV, the angle of the 2 guns at 3° and the polishing time was 15 min.

Orientation Imaging Microscopy (OIM™) was carried out using a scanning electron microscope FEG-SEM SUPRA 55 VP operating at 20 kV. The EBSD step size was 0.1 μm and 40 nm for Al1050 and AZ31 layers, respectively. The grain size data were obtained using a grain tolerance angle of 5° and the minimum grain size was chosen to be 5 pixels.All data points with a confidence index (CI) lower than 0.05 were excluded from the analysis as dubious (the CI quantifies the reliability of the indexed pattern).

The global texture of the samples was determined through neutron diffraction measurements at the Léon Brillouin Laboratory (CEA, Saclay, France) on the 6T1 goniometer in the rolling plane of the sheet. A set of three pole figures ({111}, {200}, and {220}) for Al 1050 alloy and six pole figures ({10-10}, {0002}, {10-11}, {10-12}, {11-20}, {10-13}) for AZ31 alloy were used to calculate the Orientation Distribution Function (ODF) using Mtex software [22].

X-ray diffraction (XRD) patterns were recorded on TD-ND plane of ARB deformed sampleswith the X'PERT PRO MPD diffractometer operating at 40 kV and 40 mA, using Cu-Kα radiation and fitted with the X'Celerator detector. The data were collected over a range of 20–120° in 2θ with a step size of 0.026° in 2θ andscan speed of 0.18°/*sec*. The volume fraction of precipitates was determined from a quantitative analysis using MAUD (for Material Analysis Using Diffraction, http://www.ing.untin.it/~luttero/) software.

Vickers microhardness was measured on RD-ND plane of ARB deformed samples using SHIMADZU micro-hardness tester with a load of 100 g ($Hv_{0.1}$) and indentation time of 10 s. Microhardness was measured, either on AZ31 and Al 1050 layers, at 9 different points on the strips in a cross-section line for each sample. Erroneous results were disregarded, and the mean hardness value with standard deviation error was calculated using the remaining values. The indents were spaced out by a distance of > 50 times the indentation depth in order to avoid any effect of the plastically deformed area around them.

Tensile tests were carried out using an MTS Criterion™ facility, model C45 105Zwick at room temperature to failure with strain rate of $10^{-4}\,s^{-1}$. Flat specimens with gauge dimensions of 6 mm × 12 mm were machined from the RD-TD plane of the deformed samples.

3. Results and Discussion

3.1. Microstructure Evolution of AZ31 and Al 1050 Layer After ARB Processing

Fig. 2a–e illustrate the SEM micrographs of Al 1050/AZ31/Al 1050 composite layers on the RD-ND plane after ARB processing. It can be seen that a good bonding has been obtained between AZ31 and Al 1050 layer after 1 ARB cycle. A good bonding has been also obtained between Al1050/Al1050 interfaces during the second ARB cycle, since these new formed interfaces cannot be distinguished in Fig. 2b. Similar observations and an almost homogenous deformation of the AZ31 and Al 1050 layers can be clearly seen until 4 ARB cycle as shown in Fig. 2d. A wavy structure was formed after 5 ARB cycles in which the AZ31 layers began to neck and fracture locally as shown by the arrows in Fig. 2e. Actually, the necking is located in the outer AZ31 layers and seems to be aligned at 45° to the rolling direction. The different flow properties between AZ31 and Al 1050 alloys are thought to cause plastic instabilities during the co-deformation of both alloys and as result the harder alloy (AZ31)

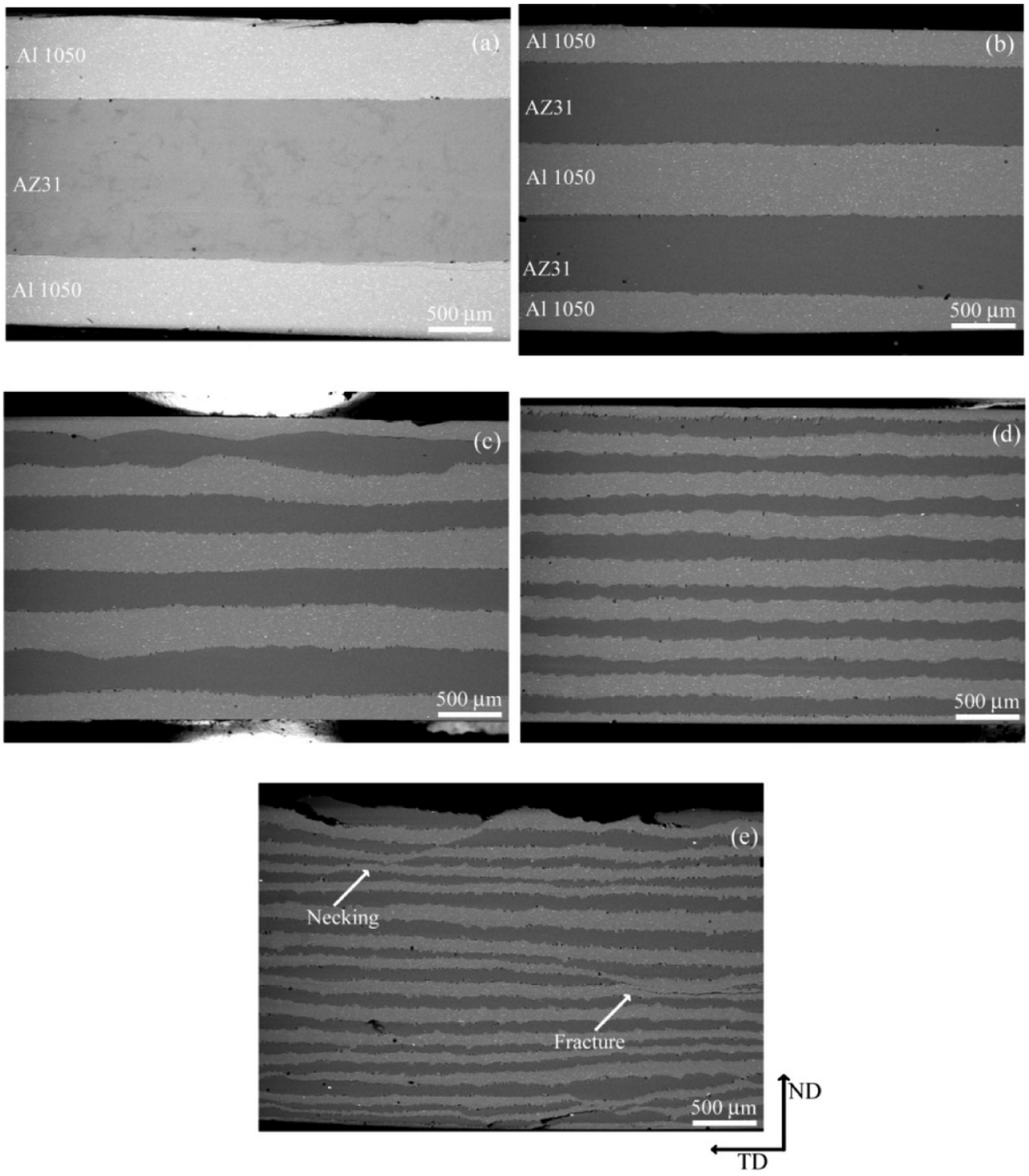

Fig. 2. SEM micrographs of Al 1050/AZ31/Al1050 laminated composite on the RD-ND plane after ARB processing: a) 1 cycle, b) 2 cycles, c) 3 cycles, d) 4 cycles, e) 5 cycles.

undergoes a necking and finally cracks [23,24]. In fact, a better bonding was successfully obtained in the present study comparatively to Al 1052/pure Mg/Al1050 [18] and Al1060/AZ31/Al1060 [20] laminated composite fabricated in quite similar ARB conditions where the fracture and necking have been observed after 4 ARB cycles.

Indeed, the thickness of both AZ31 and Al 1050 layers decreased gradually with increasing ARB cycles and they become similar after four ARB cycle as can be demonstrated in Fig. 3. As a matter of fact, at initial ARB cycles the Al 1050 layers have a half thickness of AZ31 ones, but they got similar after 3 ARB cycle. Such decrease in the thickness arose from the strong influence of the interface and the stress imposed by Al 1050 layers on the AZ31 ones [14] causing the formation of shear bands close to the interface during the rolling process. The shear band formation arises from the differences in flow strength of laminated hard and soft layers. Since it experiences the same load during rolling, the soft layer (Al1050) is subjected to higher strains than the harder layer (AZ31), which results in an in-plane shear force at the interface. Hence, the surface of Al1050 layer underwent higher strains than AZ31. This

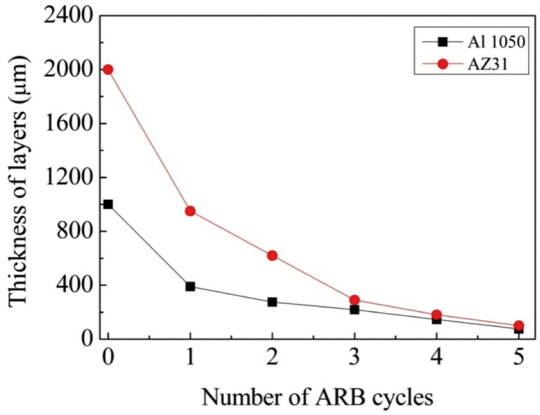

Fig. 3. Thickness variations of AZ31 and Al 1050 layers in Al 1050/AZ31/Al 1050 composite during ARB processing.

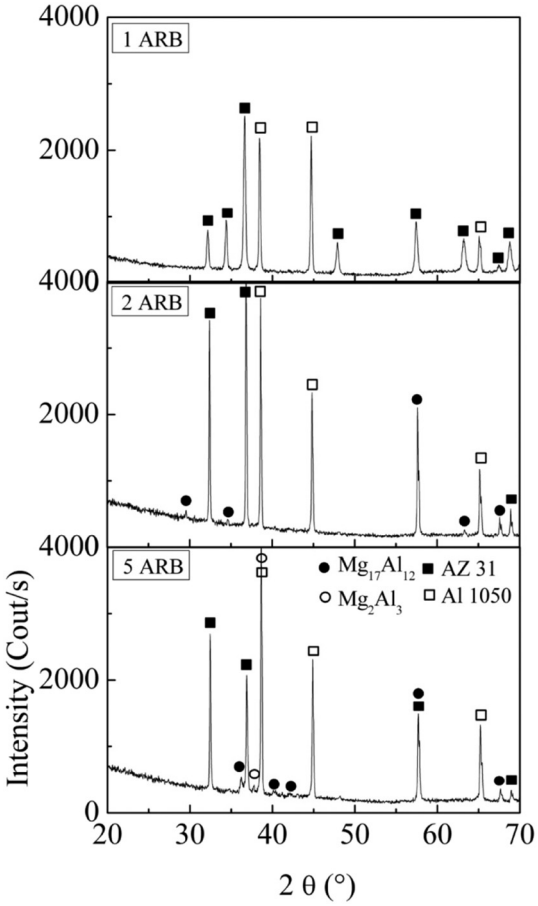

Fig. 4. XRD patterns of Al 1050/AZ31/Al 1050 laminated composite on the TD-ND plane after 1, 2 a) 1, b) 2 and c) 5 ARB cycles.

explains the fact that consequently, the thickness became close upon increasing ARB cycles [20].

The possible new phase formation near the interfaces of the laminates has been investigated by XRD. Fig. 4 presents the XRD patterns of Al 1050/AZ31/Al 1050 composite layers on the TD-ND plane after 1, 2 and 5 ARB cycles, respectively. The XRD patterns of sample after 1 ARB cycle revealed the presence of only Al and Mg phases. While, after 2 ARB cycles, new peaks appeared beside the Al and Mg phase indexed as belonging to the $Mg_{17}Al_{12}$ intermetallic compound. The volume fraction of $Mg_{17}Al_{12}$ compound was found to be around 3.3%. A new intermetallic compound with very small fraction ~ 0.3% was identified as Mg_2Al_3 in the XRD patterns of sample after 5 ARB cycles. It is to be noted that the volume fraction of $Mg_{17}Al_{12}$ compound decreased to 1.1% after 5 ARB cycles. However, as shown from the XRD patterns the different precipitate peaks have very small intensities and could be obscured in the background. Liu et al. [12] reported that the diffusion zone near the interface consisted of Mg_2Al_3 phase on the Al1050 side and $Mg_{17}Al_{12}$ phase on the AZ31 side [12], respectively. The formation of such intermetallic compounds ($Mg_{17}Al_{12}$ and Mg_2Al_3) is obviously attributed to elemental inter-diffusion between Al1050 and AZ31 layers.

This inter-diffusion involves three main mechanisms that are (1) thermally activated Al and Mg species transfer through the layers, (2) chemically induced formation reaction of the new phases due to the favorable concentration of Al and Mg atoms in the vicinity of the interface [25], (3) high strain introduced by SPD processing such as ARB [26]. A complicated interplay between these three mechanisms may exist. For example, many authors [27,28] stated that, under high pressure, the bulk diffusion coefficient may drop by about 2–3 orders of magnitude, the grain boundary (GB) diffusivity decreases by 8–15 orders of magnitude and the GB mobility becomes 2–8 orders of magnitude lower.

Figs. 5 and 6 show the orientation imaging micrographs (OIM) in inverse pole figure (IPF) mode of AZ31 and Al 1050 layers after ARB processing up to 5 cycles, respectively. The high-angle grain boundaries (HAGBs) with > 15° misorientations are presented in black, and the low-angle grain boundaries (LAGBs) are in white. It is to be noted that the black areas present in different microstructures correspond to the zones with CI values lower than 0.05 and may be attributed to the highly deformed areas near the interfaces of the laminates. As shown in Fig. 5, grains remain equiaxed during ARB. No evidence of twinning was detected in AZ31 layers. The suppression of twinning could be attributed to the grain refinement of AZ31 layers [29] and relatively high deformation temperature [30]. A rapid decrease in grain size occurs just after 1 ARB cycle, from 18 μm for the as-received alloy to 2.5 μm after 1 ARB cycle. As shown in Fig. 7a, the average grain size of AZ31 layer decreases continuously with increasing number of ARB cycles to reach a value of 0.8 μm after 5 ARB cycles. However, a relatively bimodal distribution of the grain size could be observed in the microstructure of AZ31 layer, especially for high ARB cycles (4 and 5 cycles) and could be associated to dynamic recrystallization [17]. A similar grain refinement (< 1 μm) of Mg layer after 4 ARB cycle in Al/Mg laminated composite was reported by Bing et al. [17].

In contrast, as shown in Fig. 6 after ARB processing, the grains of Al 1050 layers exhibit a typical lamellar morphology parallel to the rolling direction in line with previous studies [20,21]. However, a large grains size gradient that increased after 4 ARB cycles can be observed after ARB processing. The values of the mean spacing of HAGBs along ND (l) versus the number of ARB cycles are illustrated in Fig. 7b. The mean spacing along ND after 1 ARB cycle was about 12 μm and shows a continuous decrease to reach a value of 4.5 μm after 4 ARB cycle and then saturated (l = 4 μm after 5 ARB cycle). Jinfeng et al. [20] reported that grains in the centre of Al layers (10 μm after 4 ARB cycle) were much coarser than those in the surface layers (2 μm after 4ARB cycle).

The evolution of HAGB fraction in the microstructures of AZ31 and Al 1050 layers after ARB processing are presented in Fig. 7a and b, respectively. The HAGBs in the AZ31 layers seem to not vary considerably during ARB processing (between 35 and 40%). Meanwhile, the fraction of HAGBs in Al 1050 layers increases slowly between 1 and 2 ARB cycles (from 13 to 15%, respectively) and then a rapid increase can be noticed after 3ARB cycles to saturate after 4 ARB cycle (~23%). However, a large fraction of LAGBs remains in the microstructure of Al1050 layer even after 5 ARB cycle (~75%). This may be attributed to the continuous introduction of dislocations during the accumulative roll bonding process [31,32].

Actually, the grain refinement mechanisms are not the same in HCP and FCC metals. In HCP metals, the mechanism results mostly from dynamic recrystallization process [33,34]. In this process, new finer grains are formed along the grain boundaries of the initial coarser structure leading to the development of bimodal grain structures (as shown in Fig. 5), and these finer grains gradually consume the larger grains with increasing straining and thereby produce an ultrafine structure [35,36]. Meanwhile, in FCC metals, the mechanism of grain refinement is characterized by the transformation of LAGBs to HAGBs with subsequent increase in strain [21,31]. However, grain refinement in FCC metals may also be correlated with dynamic recrystallization, which occurs in this case when high strains cause a decrease in LAGBs and an increase in HAGBs [37,38].

3.2. Texture Evolution of AZ31 and Al 1050 Layer After ARB Processing

3.2.1. Texture Evolution of AZ31 Layers

Fig. 8 shows the texture evolution of AZ31 layers in Al 1050/AZ31/Al1050 laminated composite in term of recalculated (0002) pole figure. The texture of the as received AZ31alloy was of basal type with basal

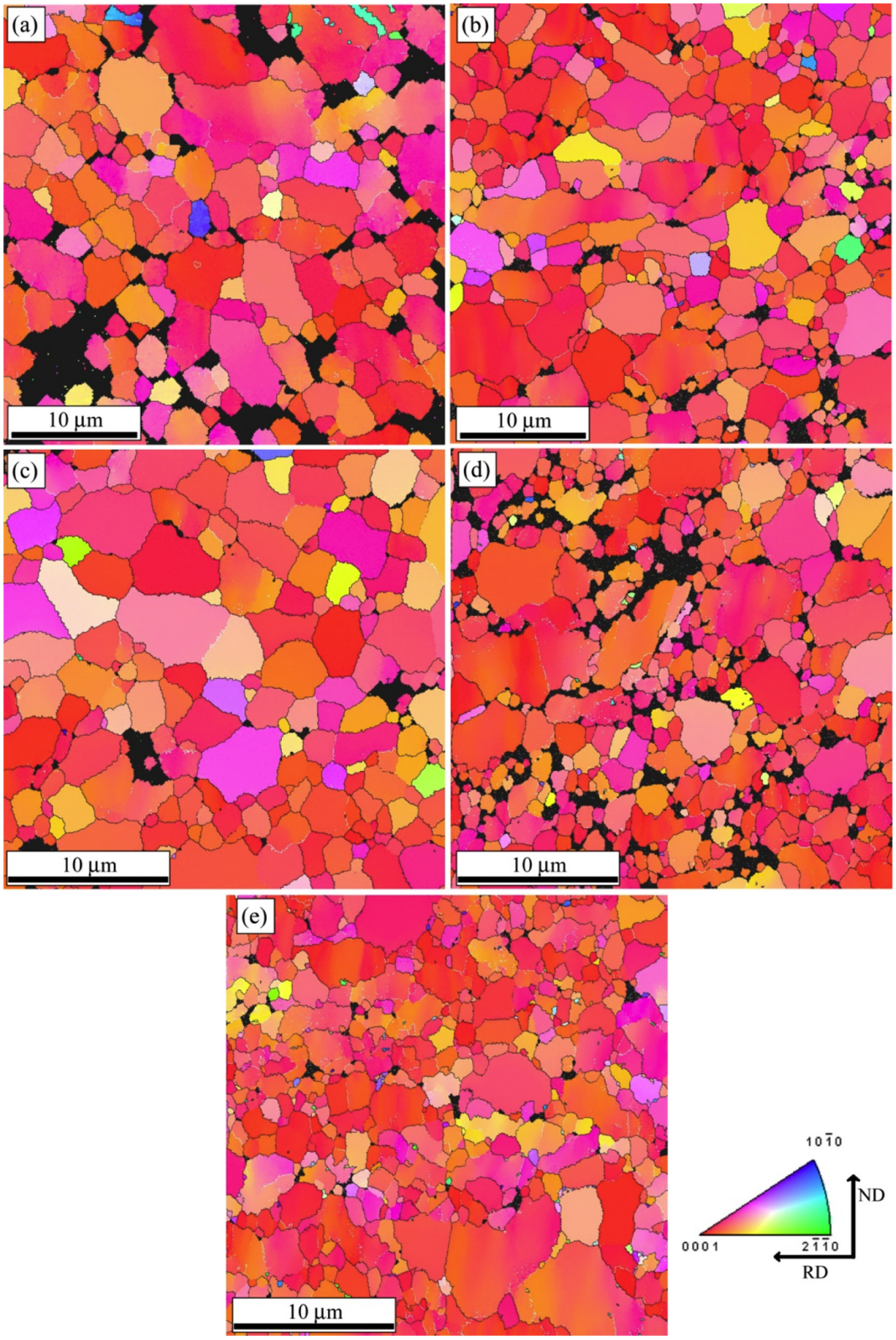

Fig. 5. IPF maps showing the microstructure evolution of AZ31 layers after ARB processing: a) 1 cycle, b) 2 cycles, c) 3 cycles, d) 4 cycles, e) 5 cycles. ⟨hkil⟩//ND.

poles tilting slightly away from normal direction (ND) towards transversal direction (TD). After ARB processing, the intensity of basal texture of AZ31 layers increases with increasing ARB cycles and the basal pole tilts away from normal direction towards rolling direction (RD). Such texture evolution of Mg layers has been already reported in hot rolled [39] or monolithic ARB Mg based alloys [40,41] and the ARBed Mg/Al laminated composite [18,19].Therefore, the co-deformation of AZ31 layers and Al 1050 layers seem to have no influence on the resulting texture in AZ31 layers.

It is interesting to estimate the texture strength index from the following equation [42]:

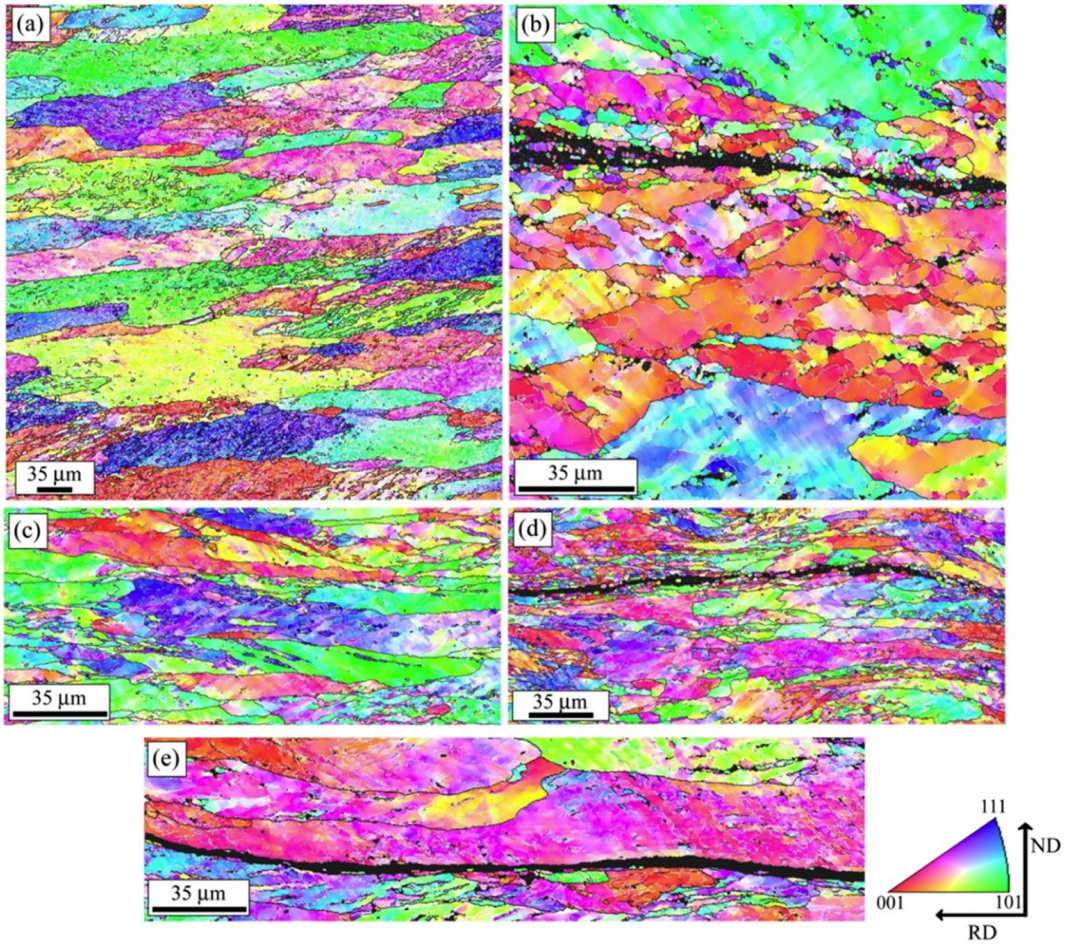

Fig. 6. IPF maps showing the microstructure evolution of Al 1050 layers after ARB processing: a) 1 cycle, b) 2 cycles, c) 3 cycles, d) 4 cycles, e) 5 cycles. ⟨hkl⟩//ND.

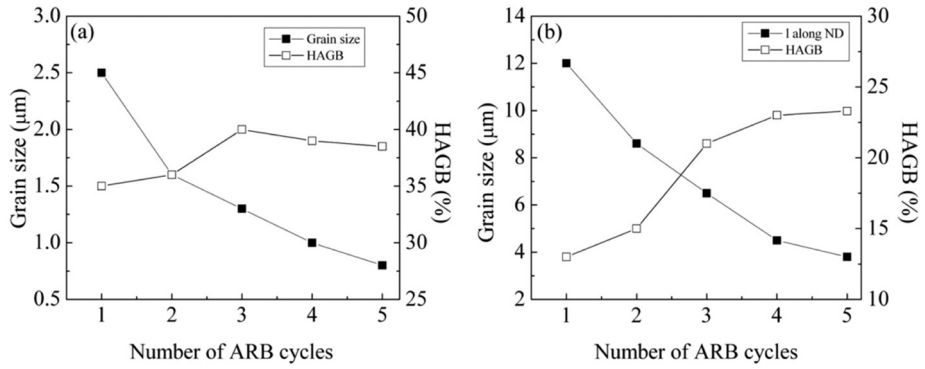

Fig. 7. Evolution of the mean spacing of HAGB along ND (*l*) and HAGB fraction with number of ARB cycle of a) AZ31 layers and b) Al 1050 layers.

$$I = \frac{1}{8\pi^2}\int_G f^2(g)dg \quad (1)$$

where $f(g)$ is the ODF values and G is the Euler space.

The strength of deformation texture is plotted against the number of ARB cycles in Fig. 9. As can be seen the strength of basal texture firstly increases and then decreases after 1 ARB cycle. The decrease of texture strength could be attributed to the dynamic recrystallization where the dynamically recrystallized grains may present more favorable orientations for basal slip, and in consequence will results in texture randomization [30,40,43]. Moreover, the weakening of the texture after one ARB cycle could also be attributed to the activation of the non-basal slips, such as pyramidal ⟨c + a⟩ and the suppression of tension twinning at high temperature [30].

3.2.2. Texture Evolution of Al 1050 Layers

Fig. 10 shows the ODF sections (φ_2 = 0, 45 and 65°) of the as received and Al 1050 layers after ARB processing up to 5 cycles. The main ideal texture component positions of FCC alloys is also plotted and their descriptions are given in Table 1. For more detail, the quantitative evolution of various texture components before and during ARB processing are summarized in Fig. 11 in terms of evolution of the α-fiber, β-fiber, θ-fiber and τ-fiber.

The texture of Al 1050 alloy before ARB processing exhibits a Cube {001}⟨100⟩ component with a strong intensity of about 12 multiple random distribution (mrd). Such texture component is known as typical recrystallization texture of FCC material sheets [44]. Meanwhile, β-fiber shows the presence of an orientation near to S component (15° far)

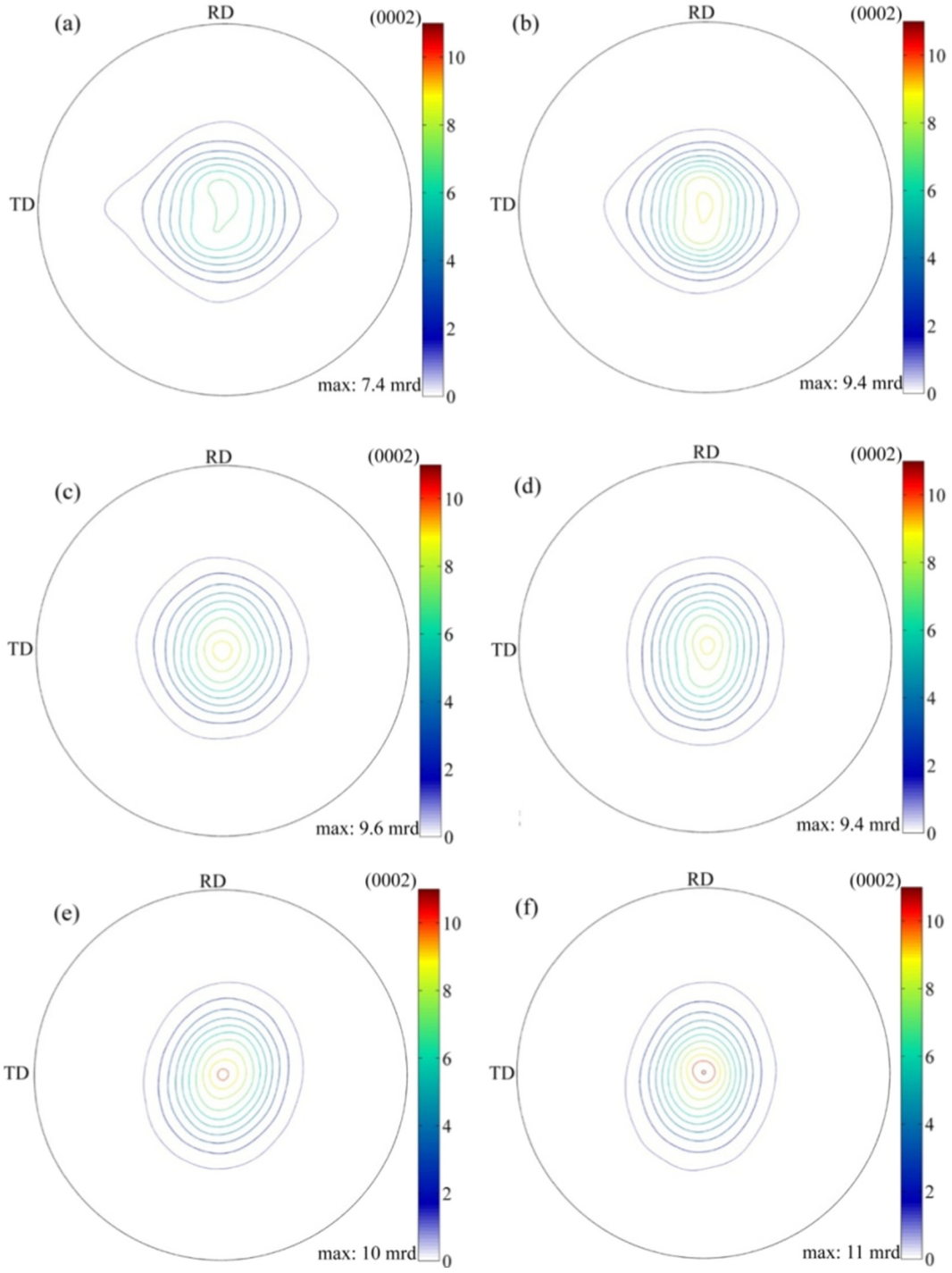

Fig. 8. Recalculated (0002) pole figures of AZ31 layers after ARB processing: a) as received, b) 1 cycle, c) 2 cycles, d) 3 cycles, e) 4 cycles and f) 5 cycles.

with intensity about 2.8 mrd. The ARB processing leads to development of relatively weak texture with the presence of Rotated Cube {001}⟨110⟩ and minor Brass {011}⟨211⟩, Copper {112}⟨111⟩ and S {123}⟨634⟩ orientations. As can be seen from Figs. 9 and 10, 1 ARB cycle leads to the formation of the Rotated Cube {001}⟨110⟩ and Copper/Dillamore components and vanishing of Cube component (~1.5 mrd from the evolution of θ-fiber). The origin of the formation of Rotated Cube was attributed to the shear strain on sheet surfaces due to frictional shear stress imposed by the rolls [21]. In fact, ARB processing of the present laminated composite was carried out without any lubricant. Therefore, a large amount of shear deformation is expected to be introduced into the surface of Al 1050 layers.

After 2 ARB cycles, no major texture evolution is observed. However, the β-fiber component intensities decrease with increasing ARB cycles and then they disappear after 5 ARB cycles leaving only a weak R-Cube component. Similar texture evolution has been reported in Al 5052 layers of pure-Mg/Al5052 laminated composite fabricated by ARB processing at 400 °C [18], except the remaining of Cube component during all ARB cycles which can be mainly attributed to the intermediate reheating during ARB process.

Usually, the intensity of rolling texture components of deformed Al alloys increases with increasing strain [45,46]. Besides, it is well established that the shear components developed in the surface of the FCC monolithic sheet processed by ARB can transform into rolling

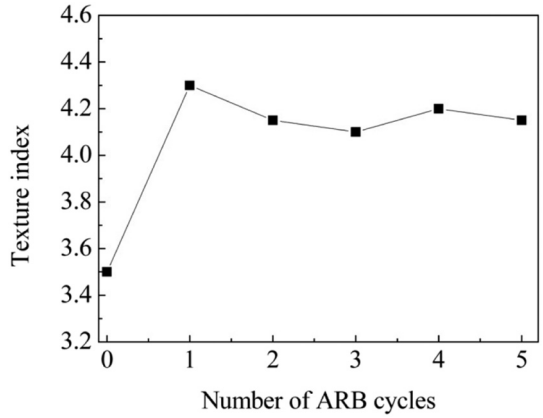

Fig. 9. Evolution of texture strength of AZ31 layers as function of number of ARB processing.

components as soon as they are transferred into the mid-thickness regions [21,47–50]. Based on the observation of Quadir et al. [51] on the microstructure evolution in ARBed Al/Al(Sc) sheets, Chang et al. [18] explained the decrease of rolling texture intensity in Al layers by the waviness structure caused by the different flowing rates of the Mg and Al layers during the roll bonding process.

However, the deformation conditions (mainly the deformation temperature) could also play a great influence on the final texture. In fact, it has been reported that the Al layer in the Mg/Al laminated composites fabricated by ARB at ambient temperature using commercial pure magnesium and Al sheets were characterized by relatively sharp β-fiber texture and Rotated Cube component [19]. Furthermore, it has been found that the fraction of Rotated Cube component increased with increasing rolling temperature in the Al/Al laminated composites fabricated by hot-roll bonding [52].

The effect of the roll-gap geometry on the inhomogeneity of microstructure and texture through the thickness of deformed sample depends on the ratio [52]:

$$\alpha = \frac{l}{h} \tag{2}$$

where l represents the projected length of contact between the rolls and the sample, and h being the mean thickness of the sample. A relatively homogeneous texture generally develops when the l/h ratio spans from 0.5 to 5 [52]. In the present work the ratio α is about 2 (l and h being 4 and 2 mm respectively), and hence the roll-gap geometry might have a large influence on resulting texture as evidenced by the domination of Rotated Cube component in Al1050 layers.

Table 1
Main ideal rolling texture components of FCC alloys.

Component	{hkl}⟨uvw⟩	Euler angle		
		φ_1	Φ	φ_2
□ Brass	{110}⟨112⟩	35°	45°	0°
◇ Goss	{110}⟨001⟩	0°	45°	0°
● Cube	{001}⟨100⟩	0°	0°	0°
○ R-Cube	{001}⟨110⟩	45°	0°	0°
△ Copper	{112}⟨111⟩	90°	35°	45°
∇ S	{231}⟨346⟩	59°	29°	63°

3.3. Mechanical Properties of Al 1050/AZ31/Al 1050 After ARB Processing

Fig. 12 illustrates the variation of microhardness of Al1050/AZ31/Al1050 laminated composite as function of number of ARB cycles. The microhardness value of the as received AZ31 and Al 1050 alloys are 54 and 42 Hv, respectively. It is well known that the hardness of the Mg layer is much higher than that of the Al layer after ARB processing [15,17,20].

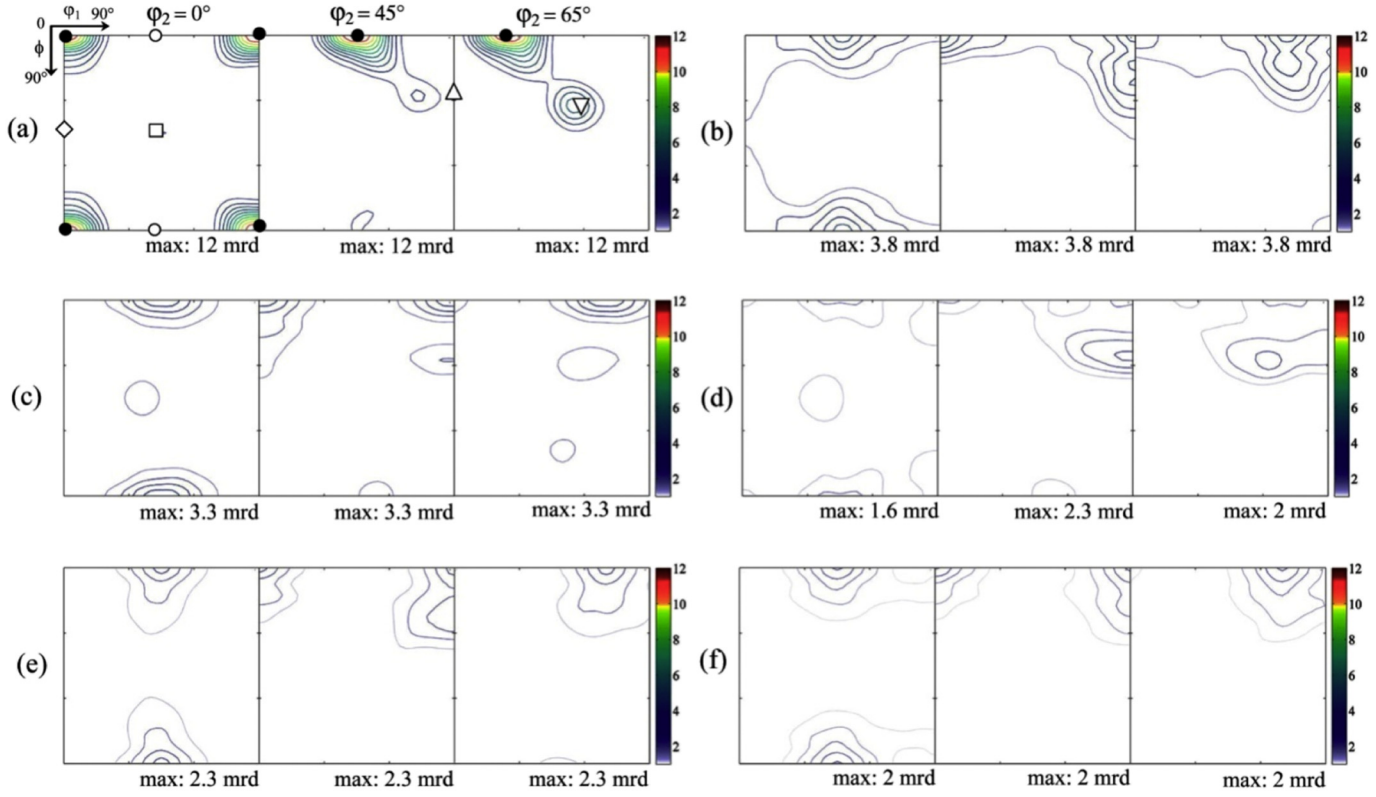

Fig. 10. ODF sections (φ_2 = 0°, 45° and 65°) obtained of Al 1050 layers after ARB processing: a) as received, b) 1 cycle, c) 2 cycles, d) 3 cycles, e) 4 cycles, f) 5 cycles.

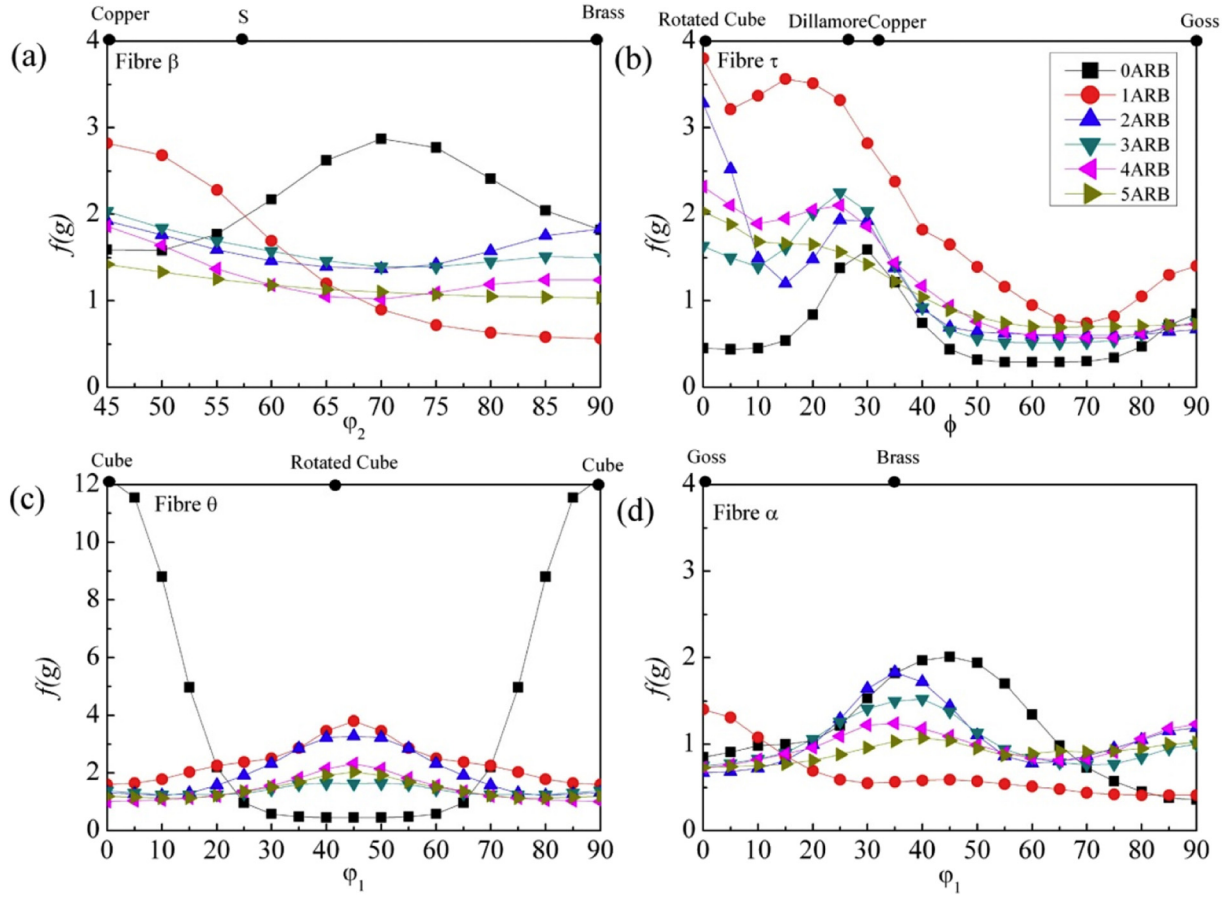

Fig. 11. Maximum intensity along the α-fiber, β-fiber, θ-fiber and τ-fiber of Al 1050 layers after ARB processing.

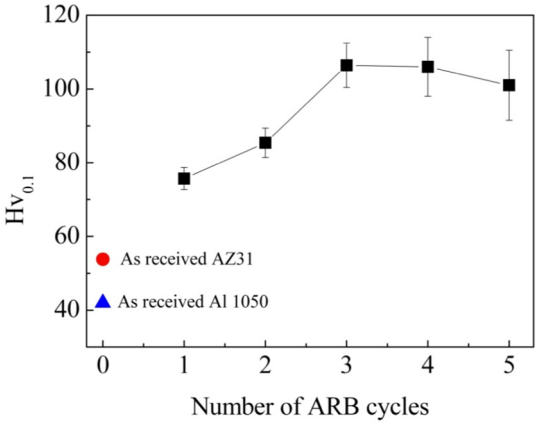

Fig. 12. Microhardness evolution of Al1050/AZ31/Al1050 laminated composite after ARB processing up to 5 cycles.

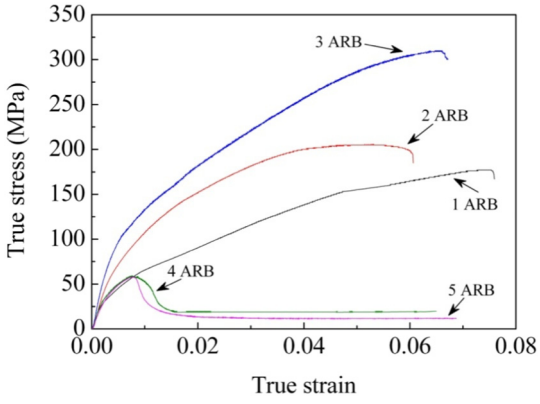

Fig. 13. True stress-true strain curves of Al1050/AZ31/Al1050 laminated composite after ARB processing up to 5 cycles.

A rapid increase of the microhardness can be observed upon increasing ARB cycles with a value about 106 Hv after 3 ARB cycles. Such an increase often accompanies the rapid increase in the dislocation density concomitant to grain refinement. The microhardness seems to reach saturation between 3 and 4 ARB cycles and then a slight decrease could be observed after 5 ARB cycles. This behavior could result from the softening behavior introduced by dynamic recrystallization.

The true stress-strain curves of Al1050/AZ31/Al1050 laminated composite after ARB processing through 5 cycles are presented in Fig.13. Tensile yield strength (TYS), ultimate tensile strength (UTS) and elongation to failure (El) of all samples extracted from the plots are listed in Table 2.

Table 2
Tensile yield strength (TYS), ultimate tensile strength (UTS) and elongation to failure (El) of Al1050/AZ31/Al 1050 laminate composite after ARB processing up to 5 cycles obtained from tensile tests:

	TYS (MPa)	UTS (MPa)	El (%)
1 ARB	40.8	177	7.8
2	48.6	206	6.2
3	104.4	310	6.9
4	47.2	59	6.8
5	46.4	58	7.1

It is clearly seen that the UTS increases rapidly from 1 ARB cycle (177 MPa) to 3 ARB cycles (310 MPa). However, as shown in Table 2, the UTS dramatically decreases after 4 and 5 ARB cycles to ~59 MPa. Similar behavior can be observed for TYS, which increases from 1 to 3 ARB cycles (from 40.8 to 104.4 MPa, respectively) and then decreases to reach a saturation value ~47.4 MPa. The elongation to failure slowly decreases and then slightly increases after 3 ARB cycles. The maximum elongation value was about 7.8% after 1 ARB cycle and the minimum value that occurred after 2 ARB cycles is around 6.2%.

The slight change in the elongation value indicates that an increasing number of ARB cycles did not improve the plasticity of the laminated composite at all. The increase of strength of Al1050/AZ31/Al1050 laminated composite between 1 and 3 ARB cycles can be attributed to the strain hardening and grain refinement of both constituents with respect to their microstructure evolution illustrated above. Moreover, it was reported that the UTS of the laminated composite depended on the relative thickness of the Al layers [53]. In the early ARB cycles, the AZ31 layers underwent deformation and elongation during tensile test because the thickness of AZ31 layers was much higher than Al1050 layers, as shown in Fig. 3. In fact, increasing number of ARB cycles (above the 4th one) reduces the Al1050 layer thicknesses which will, in turn, lower their deformation. Furthermore, the drop in UTS after 4 and 5 ARB cycles could be attributed to the brittleness of the Mg_xAl_y compounds which developed during 4 and 5 ARB cycles as demonstrated in Fig. 4. Unfortunately, in the present work the size, distribution and volume fraction of the $Mg_{17}Al_{12}$ and Mg_2Al_3 precipitates are not known accurately to confirm whether and which precipitates could influence the strain hardening. However, it is well known that the intermetallic compounds are easy to crack and fracture under large elongation deformation, and this will significantly reduce the mechanical properties of the laminated metal composites sheets [5]. A close inspection of tabulated strain-stress data in the literature indicates that YTS and UTS of Alxxxx/AZ31/Alxxxx laminated composites show same trends as those of the present study but with lower decrease at high ARB cycle numbers. Indeed, no > 10–25% decrease for both parameters between 3 and 4 ARB cycles were reported in Al5002/AZ31/Al5052 [14], Al1060/AZ31/Al1060 [20] and Al1100/AZ31/Al1100 [54] systems while an unusual collapse, i.e. > 50 and 80% decrease for YTS and UTS, is evident in the present study.

It may be interesting to note that the flow behavior after 4 and 5 ARB cycles bear a strong resemblance to those often reported in hot deformed Mg based alloy [55]. In these alloys and under such conditions, firstly, the stress rapidly increases due to work hardening, thereafter the stress reaches a peak and then decreases gradually to a steady state value indicating a significant effect of dynamic softening caused principally by dynamic recrystallization (DRX).

4. Conclusion

An Al1050/AZ31/Al1050 laminated composite was successfully fabricated through ARB processing at 400 °C, up to 5 cycles. Based on the experimental results on the evolution of microstructure, texture and mechanical properties of the Al1050/AZ31/Al1050 multilayered composites, the following conclusions are drawn:

- A good bonding has been obtained between AZ31 and Al 1050 layers. Necking and fracture of AZ31 layers took place at the final cycle (5 ARB cycle) because of the difference of the flow properties.
- XRD analysis confirmed the formation of $Mg_{17}Al_{12}$ and Mg_2Al_3 phases near the interface bonding but only after the second ARB cycle.
- Microstructure of AZ31 layers was characterized by fine equiaxed grains. The average grain size was about 0.8 μm after 5 ARB cycles. Meanwhile, the microstructure of Al 1050 layers contained elongated grains parallel to rolling direction. The values of the mean spacing of HAGB along ND was $l = 4$ μm after 5 ARB cycles.
- HAGBs fraction exhibited more or less a similar evolution in both layers. Firstly the HAGBs fraction increased with increasing strain and then saturates.
- A typical strong basal (0002) texture has been observed in AZ31 layers and a weak rolling texture showed in Al 1050 layers with domination of Rotated Cube {001}⟨110⟩ component.
- The microhardness of laminated composite increased significantly with increasing ARB cycles due to the increase of dislocation density and grain refinement. Then, the microhardness seemed to reach saturation due to a softening behavior caused by dynamic recrystallization.
- The yield strength and ultimate strength increased gradually between 1 and 3 ARB cycles due to the strain hardening and grain refinement while they decreased with further increasing of the ARB cycles because of crack and failure due to the brittleness of the Mg_xAl_y intermetallic compounds which developed during 4th and 5th ARB. The deformation behavior of the laminated composite became rather similar to the behavior of AZ31 that underwent a dynamic recrystallization during processing.
- Increasing number of ARB cycles did not improve the plasticity of the composite laminates.
- The results indicated that ARB is an effective method for producing Al1050/AZ31/Al 1050 laminated composite with advantageous mechanical properties up to three cycles.

Acknowledgements

The authors are deeply grateful to Dr-Ing. Norbert Hort and Dr. Dietmar Letzig from MagIC - Magnesium Innovations Center, Germany, for kindly providing the AZ31 alloy. Thanks to Prof. N. Bouaouadja from Sétif 1 University, Algeria, for the help and assistance during tensile tests. This work was supported in part by the international PHC-MAGHREB program No. 16MAG03.

Data Availability

The raw/processed data required to reproduce these findings cannot be shared at this time as the data also forms part of an ongoing study.

References

[1] J. Hirsch, T. Al-Samman, Superior light metals by texture engineering: optimized aluminum and magnesium alloys for automotive applications, Acta Mater. 61 (2013) 818–843, https://doi.org/10.1016/j.actamat.2012.10.044.
[2] B.L. Mordike, T. Ebert, Magnesium: properties-applications potential, Mater. Sci. Eng. A 302 (2001) 37–45, https://doi.org/10.1016/S0921-5093(00)01351-4.
[3] X. Huang, K. Suzuki, Y. Chino, M. Mabuchi, Influence of aluminum content on the texture and sheet formability of AM series magnesium alloys, Mater. Sci. Eng. A 633 (2015) 144–153, https://doi.org/10.1016/j.msea.2015.03.018.
[4] F.C. Liu, W. Liang, X.R. Li, Improvement of corrosion resistance of pure magnesium via vacuum pack treatment, J. Alloys Compd. 461 (2008) 399–403, https://doi.org/10.1016/j.jallcom.2007.06.097.
[5] Z.J. Chen, Q. Liu, G.J. Wang, D.M. Wang, Deformation in homogeneities of Mg–Al laminated metal composites fabricated by accumulative roll bonding, Mater. Res. Innov. 19 (2015) 147–151, https://doi.org/10.1179/1432891715Z.0000000001533.
[6] X.P. Zhang, S. Castagne, T.H. Yang, C.F. Gu, J.T. Wang, Entrance analysis of 7075 Al/Mg–Gd–Y–Zr/7075 Al laminated composite prepared by hot rolling and its mechanical properties, Mater. Des. 32 (2011) 1152–1158, https://doi.org/10.1016/j.matdes.2010.10.030.
[7] X.P. Zhang, T.H. Yang, S. Castagne, J.T. Wang, Microstructure; bonding strength and thickness ratio of Al/Mg/Al alloy laminated composites prepared by hot rolling, Mater. Sci. Eng. A 528 (2011) 1954–1960, https://doi.org/10.1016/j.msea.2010.10.105.
[8] C. Luo, W. Liang, Z. Chen, J. Zhang, C. Chi, F. Yang, Effect of high temperature annealing and subsequent hot rolling on microstructural evolution at the bond-interface of Al/Mg/Al alloy laminated composites, Mater. Charact. 84 (2013) 34–40 DOI https://doi.org/10.1016/j.matchar.2013.07.007.
[9] Changzeng Luo, Wei Liang, Xianrong Li, Yajun Yao, Study on interface characteristics of al/mg/al composite plates fabricated by two-pass hot rolling, Mater. Sc. Forum 747–748 (2013) 346–351, https://doi.org/10.4028/www.scientific.net/MSF.747-748.346.
[10] B. Zhu, W. Liang, X. Li, Interfacial microstructure, bonding strength and fracture of

magnesium–aluminum laminated composite plates fabricated by direct hot pressing, Mater. Sci. Eng. A 528 (2011) 6584–6588, https://doi.org/10.1016/j.msea.2011.05.015.
[11] J.H. Bae, A.K.P. Rao, K.H. Kimc, N.J. Kim, Cladding of Mg alloy with Al by twin-roll casting, Scr. Mater. 64 (2011) 836–839, https://doi.org/10.1016/j.scriptamat.2011.01.013.
[12] X.B. Liu, R.S. Chena, E.H. Han, Preliminary investigations on the Mg–Al–Zn/Al laminated composite fabricated by equal channel angular extrusion, J. Mater. Process. Technol. 209 (2009) 4675–4681, https://doi.org/10.1016/j.jmatprotec.2008.11.034.
[13] M. Kawasaki, B. Ahn, H. Lee, A. Zhilyaev, T.G. Langdon, Using high-pressure torsion to process an aluminum–magnesium nanocomposite through diffusion bonding, J. Mater. Res. 31 (2016) 88–99, https://doi.org/10.1557/jmr.2015.257.
[14] K. Wu, H. Chang, E. Maawad, W.M. Gan, H.G. Brokmeier, M.Y. Zheng, Microstructure and mechanical properties of the Mg/Al laminated composite fabricated by accumulative roll bonding (ARB), Mater. Sci. Eng. A 527 (2010) 3073–3078, https://doi.org/10.1016/j.msea.2010.02.001.
[15] H.S. Liu, B. Zhang, G.P. Zhang, Microstructures and mechanical properties of Al/Mg alloy multilayered composites produced by accumulative roll bonding, J. Mater. Sci. Technol. 27 (2011) 15–21 DOI https://doi.org/10.1016/S1005-0302(11)60019-4.
[16] H. Chang, M.Y. Zheng, C. Xu, G.D. Fan, H.G. Brokmeier, K. Wu, Microstructure and mechanical properties of the Mg/Al multilayer fabricated by accumulative roll bonding (ARB) at ambient temperature, Mater. Sci. Eng. A 543 (2012) 249–256, https://doi.org/10.1016/j.msea.2012.02.083.
[17] Zhang Bing, Chen Zhong-Wei, Yuan Shou-Qian, Zhao Tian-Li, Evolutions of microstructure for multilayered Al-Mg alloy composites by Accumulation Roll Bonding (ARB) process, Adv. Mater. Res. 411 (2012) 527–531, https://doi.org/10.4028/www.scientific.net/AMR.411.527.
[18] H. Chang, M.Y. Zheng, W.M. Gan, K. Wu, E. Maawad, H.G. Brokmeier, Texture evolution of the Mg/Al laminated composite fabricated by the accumulative roll bonding, Scr. Mater. 61 (2009) 717–720, https://doi.org/10.1016/j.scriptamat.2009.06.014.
[19] H. Chang, M.Y. Zheng, W.M. Gan, Chao Xu, H.G. Brokmeier, Texture evolution of the Mg/Al laminated composite by accumulative roll bonding at ambient temperature, Rare Metal Mater. Eng. 42 (2013) 441–446, https://doi.org/10.1016/S1875-5372(13)60044-2.
[20] J. Nie, M. Liu, F. Wang, Y. Zhao, Y. Li, Y. Cao, Y. Zhu, Fabrication of Al/Mg/Al composites via accumulative roll bonding and their mechanical properties, Materials 9 (2016) 951, https://doi.org/10.3390/ma9110951.
[21] K. Tirsatine, H. Azzeddine, T. Baudin, A.-L. Helbert, F. Brisset, B. Alili, D. Bradai, Texture and microstructure evolution of Fe-Ni alloy after accumulative roll bonding, J. Alloys Compd. 610 (2014) 352–360, https://doi.org/10.1016/j.jallcom.2014.04.173.
[22] F. Bachmann, R. Hielscher, H. Schaeben, Texture analysis with MTEX – free and open source software toolbox, Solid State Phenom. 160 (2010) 63–68, https://doi.org/10.4028/www.scientific.net/SSP.160.63.
[23] G.H. Min, J.M. Lee, S.B. Kang, H.W. Kim, Evolution of microstructure for multilayered Al/Ni composites by accumulative roll bonding process, Mater. Lett. 60 (2006) 3255–3259, https://doi.org/10.1016/j.matlet.2006.03.001.
[24] Ö. Yazar, T. Ediz, T. Öztürk, Control of macrostructure in deformation processing of metal/metal laminates, Acta Mater. 53 (2005) 375–381, https://doi.org/10.1016/j.actamat.2004.09.033.
[25] Y. Li, Liu Peng, J. Wang, H. Ma, XRD and SEM analysis near the diffusion bonding interface of Mg/Al dissimilar materials, Vacuum 82 (2008) 15–19, https://doi.org/10.1016/j.vacuum.2007.01.073.
[26] B.B. Straumal, A.R. Kilmametov, Y. Ivanisenko, A.A. Mazilkina, O.A. Kogtenkova, L. Kurmanaeva, A. Korneva, P. Zieba, B. Baretzky, Phase transitions induced by severe plastic deformation: steady-state and equifinality, Int. J. Mater. Res. 106 (2015) 657–664, https://doi.org/10.3139/146.111215.
[27] B.B. Straumal, L.M. Klinger, L.S. Shvindlerman, The influence of pressure on indium diffusion along single tin-germanium interphase boundaries, Scr. Metall. 17 (1983) 275–279, https://doi.org/10.1016/0036-9748(83)90156-4.
[28] D.A. Molodov, B.B. Straumal, L.S. Shvindlerman, The effect of pressure on migration of ⟨001⟩ tilt grain boundaries in tin bicrystals, Scr. Metall. 18 (1984) 207–211, https://doi.org/10.1016/0036-9748(84)90509-X.
[29] Y. Chino, K. Kimura, M. Mabuchi, Twinning behavior and deformation mechanisms of extruded AZ31 Mg alloy, Mater. Sci. Eng. A 486 (2008) 481–488, https://doi.org/10.1016/j.msea.2007.09.058.
[30] Y. Chino, M. Mabuchi, Enhanced stretch formability of Mg–Al–Zn alloy sheets rolled at high temperature (723 K), Scr. Mater. 60 (2009) 447–450, https://doi.org/10.1016/j.scriptamat.2008.11.029.
[31] A.Y. Khereddine, F. HadjLarbi, H. Azzeddine, T. Baudin, F. Brisset, A.L. Helbert, M.H. Mathon, M. Kawasaki, D. Bradai, T.G. Langdon, Microstructures and textures of a Cu-Ni-Si alloy processed by high-pressure torsion, J. Alloys Compd. 574 (2013) 361–367, https://doi.org/10.1016/j.jallcom.2013.05.051.
[32] M. Kawasaki, Z. Horita, T.G. Langdon, Microstructural evolution in high purity aluminum processed by ECAP, Mater. Sci. Eng. A524 (2009) 143–150, https://doi.org/10.1016/j.msea.2009.06.032.
[33] R.B. Figueiredo, T.G. Langdon, Principles of grain refinement in magnesium alloys processed by equal-channel angular pressing, J. Mater. Sci. 44 (2009) 4758–4762, https://doi.org/10.1007/s10853-009-3725-z.
[34] R.B. Figueiredo, T.G. Langdon, Grain refinement and mechanical behaviour of a magnesium alloy processed by ECAP, J. Mater. Sci. 45 (2010) 4827–4836, https://doi.org/10.1007/s10853-010-4589-y.
[35] K. Edalati, A. Yamamoto, Z. Horita, T. Ishihara, High-pressure torsion of pure magnesium: evolution of mechanical properties, microstructures and hydrogen storage capacity with equivalent strain, Scr. Mater. 64 (2011) 880–883, https://doi.org/10.1016/j.scriptamat.2011.01.023.
[36] R.B. Figueiredo, S. Sabbaghianrad, A. Giwa, J.R. Greer, T.G. Langdon, Evidence for exceptional low temperature ductility in polycrystalline magnesium processed by severe plastic deformation, Acta Mater. 122 (2017) 322–331, https://doi.org/10.1016/j.actamat.2016.09.054.
[37] T. Sakai, A. Belyakov, R. Kaibyshev, H. Miura, J.J. Jonas, Dynamic and post-dynamic recrystallization under hot, cold and severe plastic deformation conditions, Prog. Mater. Sci. 60 (2014) 130–207, https://doi.org/10.1016/j.pmatsci.2013.09.002.
[38] N.S. De Vincentis, A. Kliauga, M. Ferrante, M. Avalos, H.-G. Brokmeier, R.E. Bolmaro, Evaluation of microstructure anisotropy on room and medium temperature ECAP deformed F138 steel, Mater. Charact. 107 (2015) 98–111, https://doi.org/10.1016/j.matchar.2015.06.035.
[39] S. Abdessameud, D. Bradai, Microstructure and texture evolution in hot rolled and annealed magnesium alloy TRC AZ31, Can. Metall. Q. 48 (2009) 433–442, https://doi.org/10.1179/cmq.2009.48.4.433.
[40] M.Y. Zhan, Y.Y. Li, W.P. Chen, W.D. Chen, Microstructure and mechanical properties of Mg-Al-Zn alloy sheets severely deformed by accumulative roll-bonding, J. Mater. Sci. 42 (2007) 9256–9261, https://doi.org/10.1007/s10853-007-1885-2.
[41] F. Schwarz, K. Lange, L. Krüger, R. Kawalla, St. Reichelt, Microstructural and mechanical characterization of ARB AZ31, Mater. Sci. Forum 765 (2013) 403–407, https://doi.org/10.4028/www.scientific.net/MSF.765.403.
[42] U.F. Kocks, C.N. Tomé, H.R. Wenk, Texture and Anisotropy: Preferred Orientations in Polycrystals and Their Effect on Materials Properties, Cambridge University Press, 2000.
[43] J.A. Del Valle, M.T. Perez-Prado, O.A. Ruano, Texture evolution during large-strain hot rolling of the Mg AZ61 alloy, Mater. Sci. Eng. A 355 (2003) 68–78, https://doi.org/10.1016/S0921-5093(03)00043-1.
[44] F.J. Humphreys, M. Hatherly, Recrystallization and Related Annealing Phenomena, Second ed., Elsevier, Oxford, UK, 2004.
[45] W.C. Liu, J.G. Morris, Effect of hot and cold deformation on the β fiber rolling texture in continuous cast AA 5052 aluminum alloy, Scr. Mater. 52 (2005) 1317–1321, https://doi.org/10.1016/j.scriptamat.2005.02.031.
[46] W.C. Liu, J.G. Morris, Effect of hot and cold deformation on the recrystallization texture of continuous cast AA 5052 aluminum alloy, Scr. Mater. 53 (2005) 1273–1277, https://doi.org/10.1016/j.scriptamat.2005.07.040.
[47] G.E. Dieter, Mechanical Metallurgy, McGraw-Hill, New York, 1976.
[48] S. Roy, S.D. Singh, S. Suwas, S. Kumar, K. Chattopadhyay, Microstructure and texture evolution during accumulative roll bonding of aluminium alloy AA5086, Mater. Sci. Eng. A 528 (2011) 8469–8478, https://doi.org/10.1016/j.msea.2011.07.042.
[49] C.P. Heason, P.B. Prangnell, Texture evolution and grain refinement in Al deformed to ultra-high strains by Accumulative Roll Bonding (ARB), Mater. Sci. Forum 408–412 (2002) 733–738, https://doi.org/10.4028/www.scientific.net/MSF.408-412.733.
[50] R. Jamaati, M.R. Toroghinejad, Effect of alloy composition, stacking fault energy, second phase particles, initial thickness, and measurement position on deformation texture development of nanostructured FCC materials fabricated via accumulative roll bonding process, Mater. Sci. Eng. A 598 (2014) 77–97, https://doi.org/10.1016/j.msea.2014.01.020.
[51] M.Z. Quadir, M. Ferry, O. Al-Buhamad, P.R. Munroe, Shear banding and recrystallization texture development in a multilayered Al alloy sheet produced by accumulative roll bonding, Acta Mater. 57 (2009) 29–40, https://doi.org/10.1016/j.actamat.2008.08.056.
[52] Z.J. Wang, L. Zhai, M. Ma, H. Yuan, W.C. Liu, Microstructure, texture and mechanical properties of Al/Al laminated composites fabricated by hot rolling, Mater. Sci. Eng. A 644 (2015) 194–203, https://doi.org/10.1016/j.msea.2015.07.035.
[53] X.P. Zhang, T.H. Yang, J.Q. Liu, X.F. Luo, J.T. Wang, Mechanical properties of an Al/Mg/Al trilaminated composite fabricated by hot rolling, J. Mater. Sci. 45 (2010) 3457–3464, https://doi.org/10.1007/s10853-010-4373-z.
[54] C.C. Hsieh, M.C. Chen, W. Wu, Mechanical property and fracture behavior of Al/Mg composite produced by accumulative roll bonding technique, J. Compos. 2013 (2013) 748273, , https://doi.org/10.1155/2013/748273 (8 pages).
[55] H. Azzeddine, D. Bradai, On some aspects of compressive properties and serrated flow in Mg-Y-Nd alloy, J. Rare Earths 31 (2013) 804–810, https://doi.org/10.1016/S1002-0721(12)60362-7.